Supplementary Information

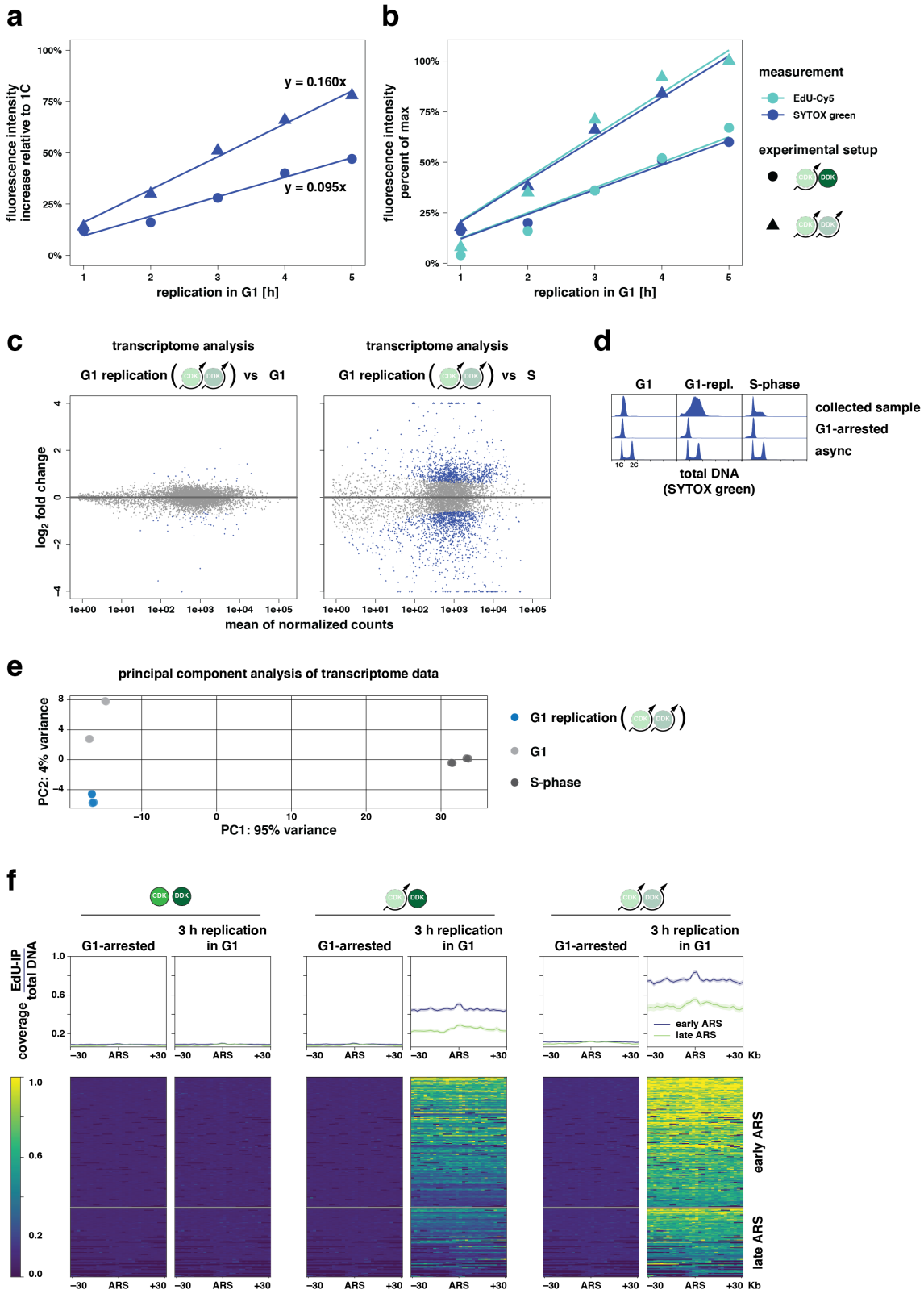

Supplementary Figure 1

Unscheduled replication in G1 initiates at canonical replication origins genome-wide

(a) DNA content increases linearly during unscheduled replication in G1. Data from Fig. 1b. Cells were arrested in G1 and replication was induced by using either CDK bypass or CDK/DDK bypass systems. Mean fluorescence intensity of total DNA (SYTOX green, blue) was measured by flow cytometry after induction of G1 replication for the indicated amount of time. Data were corrected for background mitochondrial DNA synthesis in the control strain, normalized to a DNA content of 1 C and fitted with a linear regression model (see equation).

(b) DNA is quantitatively labeled with EdU during G1 replication. Data from Fig. 1b. As in (a), additionally measuring mean fluorescence intensity of newly synthesized DNA in G1 (EdU-Cy5, turquoise). Data were corrected for background mitochondrial DNA synthesis in the control strain and normalized to the respective maximum value.

(c) and (d) and (e) Cells keep a G1-like transcriptional signature despite induction of replication and do not transit into an S-like state. Analysis of transcript abundance by mRNA-seq of control cells in G1 and S-phase as well as CDK/DDK bypass cells undergoing unscheduled replication in G1. Control cells were harvested after G1 arrest or released to S-phase; G1-replicating cells were harvested after G1 arrest followed by 3 h of replication induced by CDK/DDK bypass. Poly(A)-containing RNAs were enriched from total RNA and sequenced. (c) Comparison of the transcriptome of CDK/DDK bypass cells in G1 to control cells in G1-phase (left) or S-phase (right). The abundance of individual transcripts is plotted against their fold change in the compared conditions. Transcripts with a statistically significant log-fold change > 0.5 are colored blue. Triangles indicate transcript data that fell outside of the plotted interval. (d) Representative plots of total cellular DNA content as a proxy for cell cycle stage and DNA replication activity. DNA was stained with SYTOX green and measured by flow cytometry. (e) Principal component analysis of the dataset. Cell cycle phase explains 95% of the observed variance between the three conditions. Data from n=4 biological replicates per experimental condition

(f) Early-replicating origins are activated during G1 replication. Related to Fig. 1c. Cells were arrested in G1 and replication was induced for 3 h in the presence of 100 μM EdU. Input-normalized EdU-sequencing data were analyzed at early or late replication origins (ARS) ± 30 Kb and showed wide-spread replication. (top) Profile plots of mean coverage (dark) ± SE (light). (bottom) Heatmaps with 1 Kb bin size. Data are representative of n=2 biological replicates.

a

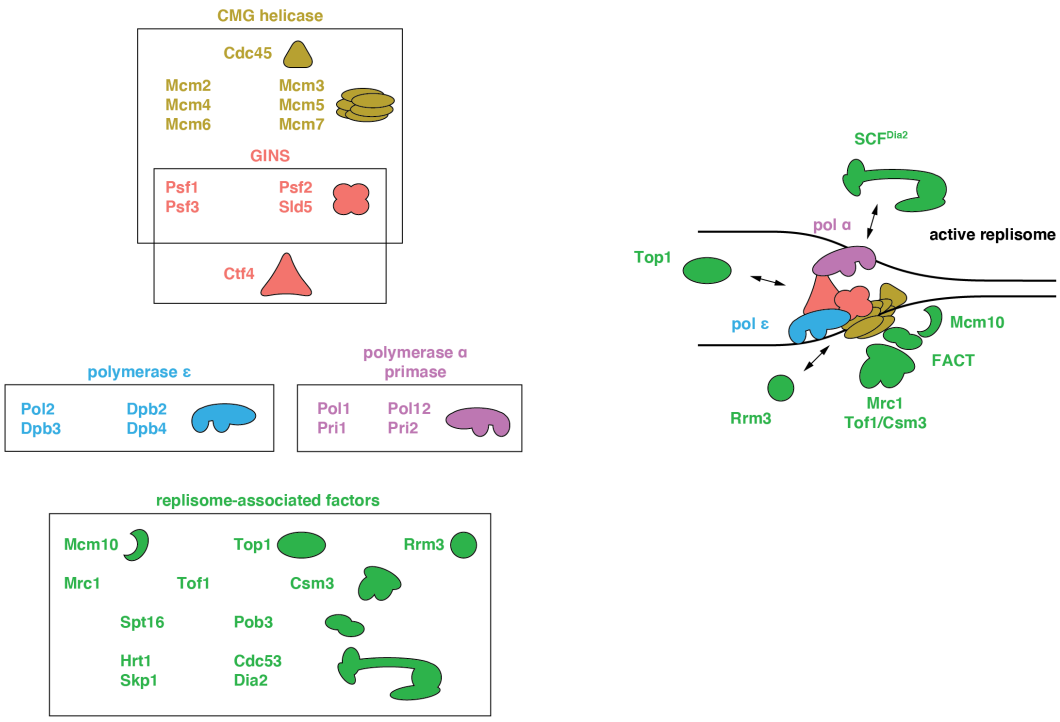

Supplementary Figure 2

Sub-complexes within the replisome

(a) Schematic drawing of a replisome and its sub-complexes. Color code as in Fig. 2. Interaction of GINS/Ctf4 with Mcm2-7/Cdc45 indicates formation of the CMG helicase, which is the key step in the transition from inactive helicase precursors to active replisomes during replication initiation. DNA polymerases and replisome-associated factors are recruited during or after this transition and travel with the replisome.

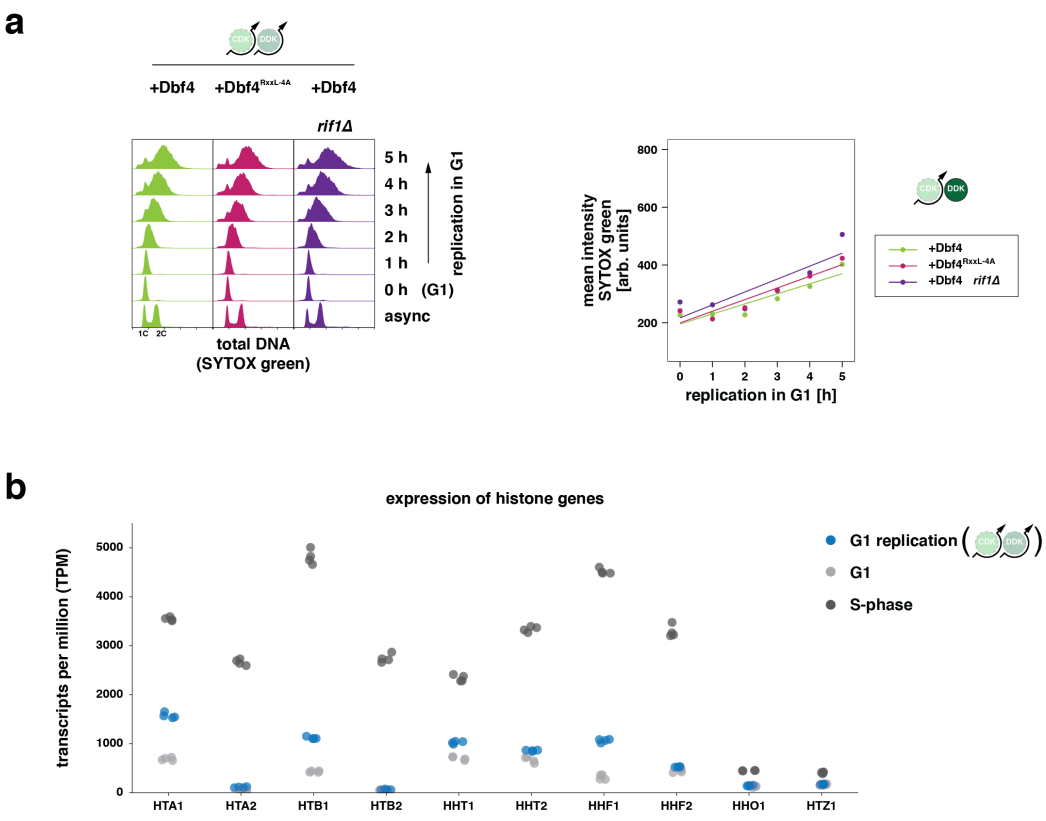

Supplementary Figure 3

Factors limiting unscheduled G1 replication

(a) Enhanced deregulation of Dbf4-dependent kinase (DDK) does not increase the amount of unscheduled replication in G1 under CDK/DDK bypass conditions. Strains expressing high levels of either *DBF4, expressing high levels of* a *DBF4* allele with mutated destruction-boxes (*dbf4*$^{RxxL-4A}$), or lacking *RIF1* (a targeting subunit for the DDK-antagonizing PP1 phosphatase) were additionally used in this experiment. (left) SYTOX green-stained total DNA as measured by flow cytometry at the indicated timepoints shows highly similar progression of unscheduled DNA replication during G1. (right) Quantification of the flow cytometry data by approximation of a bimodal distribution and calculating the means of the individual normal distributions. The average mean from 5 fits per timepoint is shown together with a linear regression. Data are representative of n=2 biological replicates.

(b) Expression of histone genes is low during G1 replication but strongly induced during early S phase. The frequency of individual histone gene transcripts (transcriptome data as analyzed in Supplementary Figure 1c-e) from cells in G1-phase, S-phase, or undergoing G1 replication, normalized for library size and transcript length. Data from n=4 biological replicates per condition.

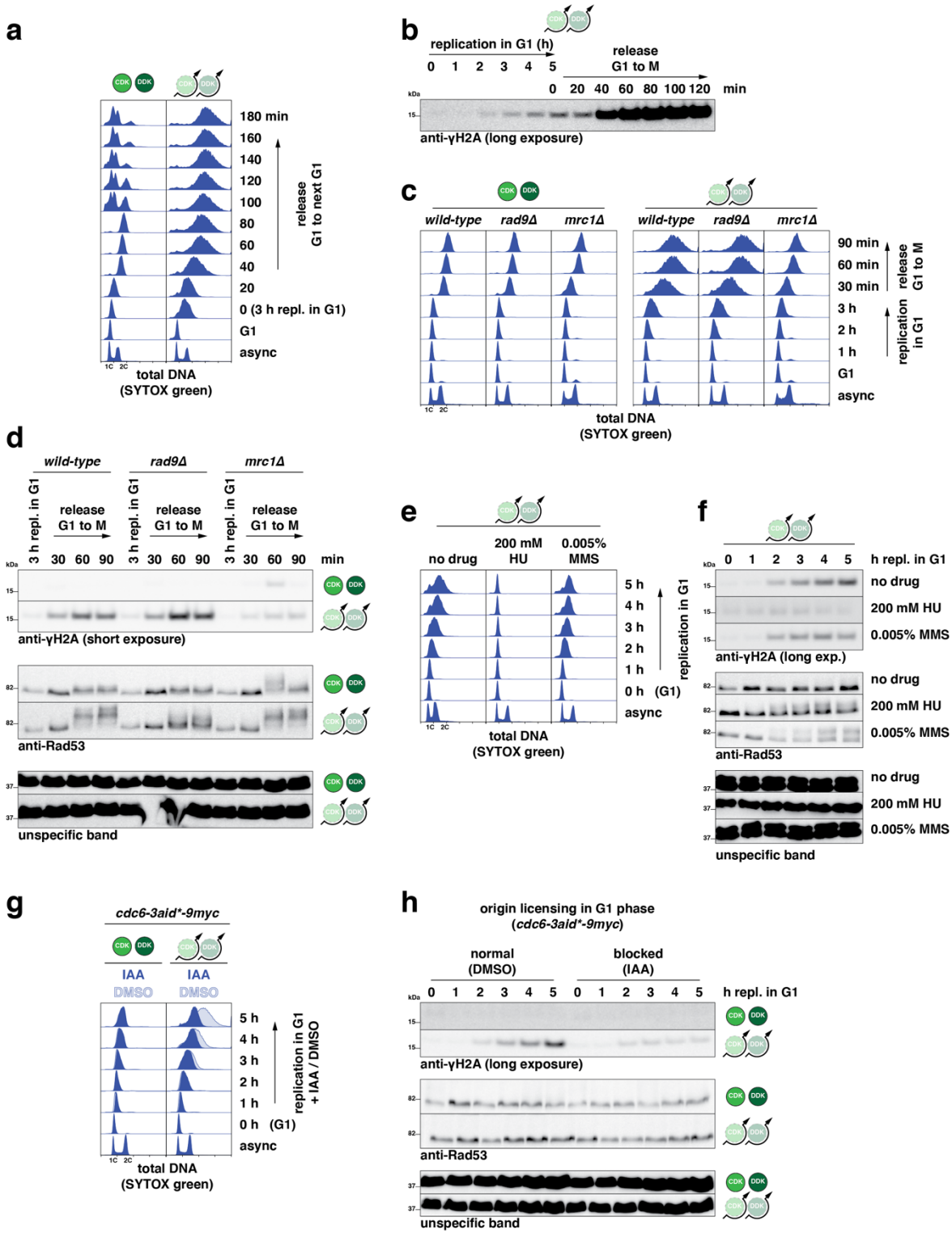
a
180 min
160
140
120
100
80
60
40
20
0 (3 h repl. in G1)
G1
async
release G1 to next G1
1C 2C
total DNA (SYTOX green)
b
replication in G1 (h)
0 1 2 3 4 5
release G1 to M
0 20 40 60 80 100 120 min
kDa
15
anti-γH2A (long exposure)
c
wild-type rad9Δ mrc1Δ
wild-type rad9Δ mrc1Δ
90 min
60 min
30 min
3 h
2 h
1 h
G1
async
release G1 to M
replication in G1
total DNA (SYTOX green)
d
wild-type rad9Δ mrc1Δ
3 h repl. in G1
release G1 to M
30 60 90 min
anti-γH2A (short exposure)
anti-Rad53
unspecific band
e
no drug
200 mM HU
0.005% MMS
5 h
4 h
3 h
2 h
1 h
0 h (G1)
async
replication in G1
total DNA (SYTOX green)
f
0 1 2 3 4 5 h repl. in G1
no drug
200 mM HU
0.005% MMS
anti-γH2A (long exp.)
anti-Rad53
unspecific band
g
cdc6-3aid*-9myc
IAA
DMSO
5 h
4 h
3 h
2 h
1 h
0 h (G1)
async
replication in G1 + IAA / DMSO
total DNA (SYTOX green)
h
origin licensing in G1 phase (cdc6-3aid*-9myc)
normal (DMSO)
blocked (IAA)
0 1 2 3 4 5 0 1 2 3 4 5 h repl. in G1
anti-γH2A (long exposure)
anti-Rad53
unspecific band

Supplementary Figure 4
Unscheduled G1 replication induces DNA damage upon subsequent S-phase replication

(a) Release from unscheduled G1 replication results in cell cycle arrest after S-phase. After 3 h of replication in G1 induced by using the CDK/DDK bypass system, cells were released to the cell cycle and arrested in the next G1-phase. Total DNA content (SYTOX green stain) was measured by flow cytometry at the indicated timepoints. Starting at 80 min control cells enter the next G1-phase, while G1 replication cells stay arrested with G2/M DNA content. Data are representative of n=2 biological replicates.

(b) Unscheduled G1 replication generates low amounts of DNA damage already in G1. Longer exposure of the γH2A western blot that is shown in Fig. 4b (representative of n=2 biological replicates).

(c) and (d) DNA damage after unscheduled replication in G1 is detected by the Rad9-dependent DNA damage checkpoint. Unscheduled replication in G1 was induced in cells deficient in Rad9 or Mrc1 checkpoint signaling factors by CDK/DDK bypass before release of the cells to nocodazole-containing medium. (c) SYTOX green-stained total DNA content as measured by flow cytometry at the indicated timepoints. (d) Western blots of samples from (c) detecting γH2A and Rad53 at the indicated timepoints. An unspecific band from the Rad53 western blots is included as a loading control. Data are representative of n=2 biological replicates.

(e) and (f) The checkpoint detects canonical replication stress (replication fork stalling) in G1-arrested cells. G1 replication was induced by the CDK/DDK bypass system, but in the presence of additional replication perturbation by hydroxyurea (HU) or methyl methanesulfonate (MMS). (e) Total DNA content (SYTOX green-stained) was measured by flow cytometry. (f) Western blots of samples from (e) detecting γH2A and Rad53 at the indicated timepoints. An unspecific band from the Rad53 western blots is included as a loading control. Data are representative of n=2 biological replicates.

(g) and (h) Generation of DNA damage in G1 requires continuous origin licensing. Replication was induced in G1-arrested cells by CDK/DDK bypass with/without concomitant depletion of licensing factor Cdc6 via an auxin-inducible degron. (g) Total DNA content (SYTOX green-stained) as measured by flow cytometry at the indicated timepoints. (h) Western blots of samples from (g) detecting γH2A and Rad53 at the indicated timepoints. An unspecific band from the Rad53 western blots is included as a loading control. Data are representative of n=2 biological replicates.

Source data are provided as a Source Data file.

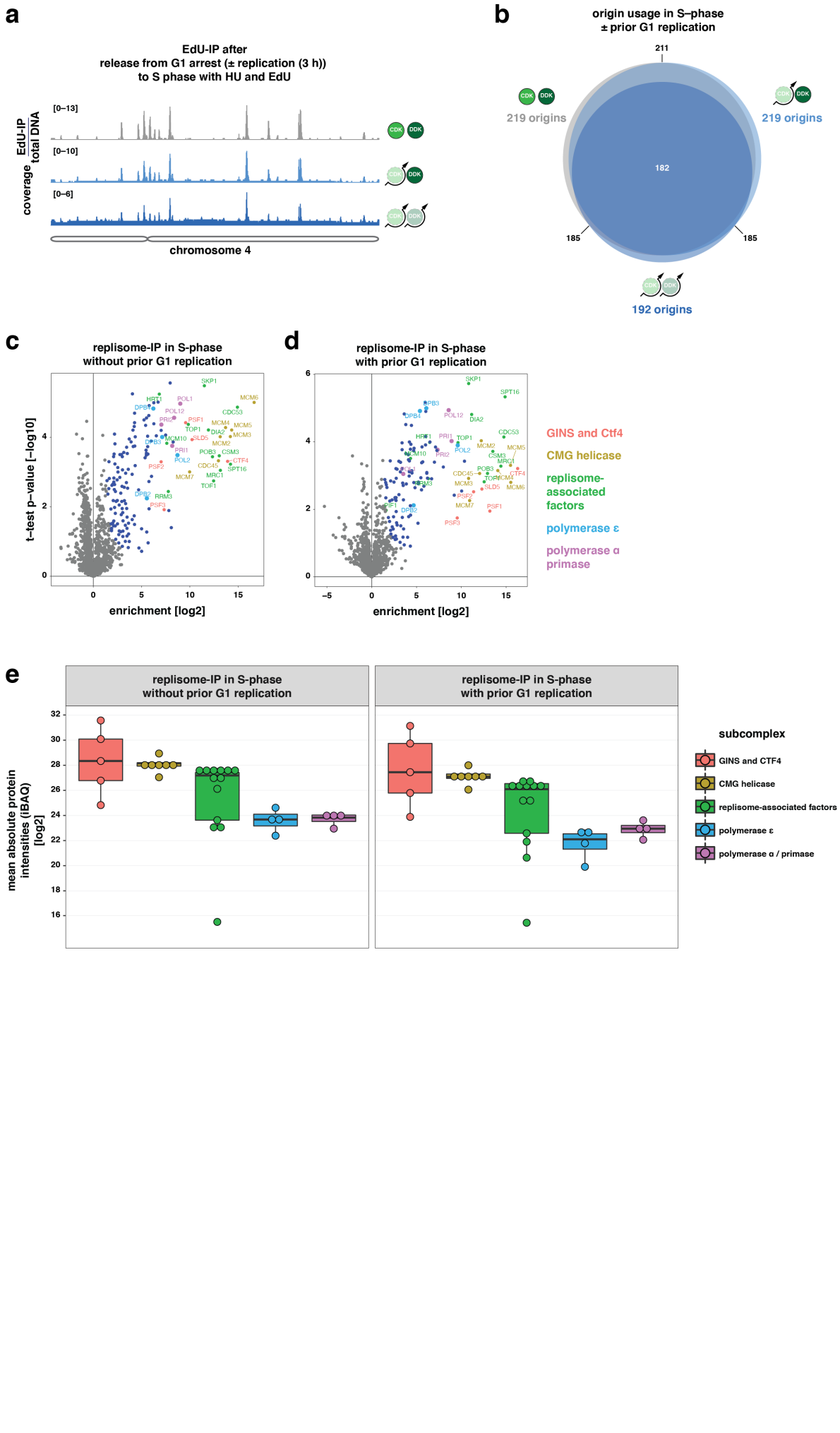
a
EdU-IP after
release from G1 arrest (± replication (3 h))
to S phase with HU and EdU
EdU-IP
total DNA
coverage
[0–13]
[0–10]
[0–6]
CDK
DDK
chromosome 4
b
origin usage in S–phase
± prior G1 replication
211
219 origins
219 origins
182
185
185
192 origins
c
replisome-IP in S-phase
without prior G1 replication
t–test p–value [–log10]
enrichment [log2]
d
replisome-IP in S-phase
with prior G1 replication
enrichment [log2]
GINS and Ctf4
CMG helicase
replisome-
associated
factors
polymerase ε
polymerase α
primase
e
replisome-IP in S-phase
without prior G1 replication
replisome-IP in S-phase
with prior G1 replication
mean absolute protein
intensities (iBAQ)
[log2]
subcomplex
GINS and CTF4
CMG helicase
replisome-associated factors
polymerase ε
polymerase α / primase

Supplementary Figure 5

G1 replication does not disturb subsequent replication initiation in S-phase

(a) Unscheduled G1 replication does not affect origin usage in the subsequent S-phase. To visualize origin usage, replication was induced in G1-arrested cells prior to release into S-phase for 90 min in the presence of 200 mM HU and 100 μM EdU. EdU-labeled DNA was isolated and sequenced. Input-normalized coverage of chromosome 4 in 1 Kb bins is shown as indicated on a linear scale. Y-axes scales are given in the top-left corners. Note the highly similar relative intensity of the peaks and the increased baseline signal in cells after G1 replication which likely is due to ongoing replication from G1 replisomes. Data are representative of n=2 biological replicates.

(b) Unscheduled G1 replication does not affect origin usage in the subsequent S-phase. Data in (a) was used to call peaks and compare between the three experimental conditions. Origins detected in S-phase in control cells are depicted in gray; origins detected in S-phase after CDK and CDK/DDK bypass are depicted in shades of blue and overlap strongly with canonical early origins of S-phase.

(c) to (e) Replisome composition in S-phase is not broadly affected by prior G1 replication. Cells were released from a G1-arrest to S-phase with or without prior induction of replication in G1 by CDK/DDK bypass. Replisomes were affinity-purified from these S-phase extracts via GFP-tagged GINS-subunit Psf2 and analyzed by mass spectrometry. (c)/(d) Volcano-plots of the enrichment of proteins in GFP-tagged samples versus untagged control samples. Colors indicate statistically significantly enriched proteins; different replisome subcomplexes are additionally highlighted as indicated. (e) Label-free quantification and comparison of the datasets shown in (c)/(d) using intensity-based absolute quantification (iBAQ). Boxes indicate the median with the first and third quartile of the sub-complexes, whiskers indicate the minimum and maximum (calculated by extending the box by 1.5 inter-quartile range). Mean iBAQ values for individual proteins are plotted as circles. Data from n=3 biological replicates.

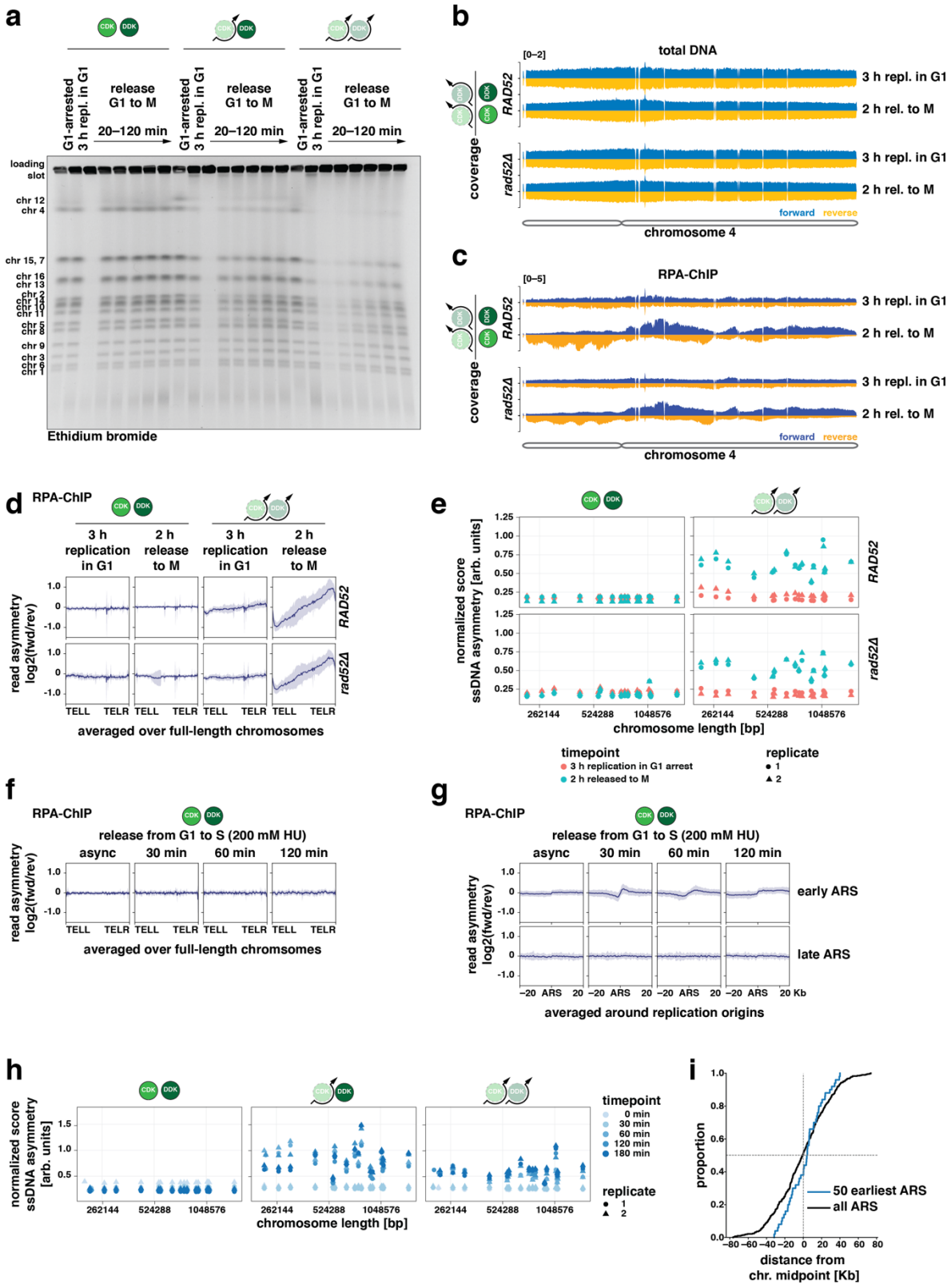
a
G1-arrested 3 h repl. in G1
release G1 to M
20–120 min
loading slot
chr 12
chr 4
chr 15, 7
chr 16
chr 13
chr 2
chr 14
chr 10
chr 11
chr 5
chr 8
chr 9
chr 3
chr 6
chr 1
Ethidium bromide
b
total DNA
[0–2]
RAD52
rad52Δ
coverage
3 h repl. in G1
2 h rel. to M
forward
reverse
chromosome 4
c
RPA-ChIP
[0–5]
d
RPA-ChIP
3 h replication in G1
2 h release to M
read asymmetry log2(fwd/rev)
TELL
TELR
averaged over full-length chromosomes
e
normalized score ssDNA asymmetry [arb. units]
262144
524288
1048576
chromosome length [bp]
timepoint
3 h replication in G1 arrest
2 h released to M
replicate
f
RPA-ChIP
release from G1 to S (200 mM HU)
async
30 min
60 min
120 min
averaged over full-length chromsomes
g
averaged around replication origins
early ARS
late ARS
ARS
Kb
h
timepoint
0 min
30 min
60 min
120 min
180 min
i
proportion
50 earliest ARS
all ARS
distance from chr. midpoint [Kb]

Supplementary Figure 6
Successive G1 and S replication generate single-ended DSBs from head-to-tail-fork collisions, resulting in an asymmetric pattern of RPA-bound ssDNA on chromosome arms

(a) Persistent replication/repair structures after release from unscheduled G1 replication. Ethidium bromide-stained gel after pulsed-field gel electrophoresis corresponding to Fig. 5a. Samples were taken at the indicated timepoints after inducing G1 replication and released to nocodazole-containing medium and separated on a pulsed-field electrophoresis gel. Data are representative of n=2 biological replicates.

(b) to (e) The strand-biased accumulation of RPA (indicating single-stranded DNA) does not depend on *RAD52* excluding break-induced replication as a causative factor. Cells were arrested in G1, replication was induced for 3 h, and cells were subsequently released to nocodazole-containing medium. Samples were crosslinked at the indicated times and RPA-bound DNA was purified for sequencing. Single-stranded DNA (as indicated by RPA binding) accumulated similarly in the absence and presence of recombination factor Rad52. (b) and (c) show representative coverage traces of reads mapping to chromosome 4 for total DNA (b) and RPA-ChIP (c) of strains with and without *RAD52*. The scale of the y-axes is indicated in the top-left corner of the panels. (d) The read asymmetry (log2-ratio of RPA-ChIP-seq reads mapping to forward and reverse strands) was averaged over full-length chromosomes at the indicated timepoints and plotted as mean (dark) ± SD (light). (e) single-stranded DNA (ssDNA) asymmetry scores for individual chromosomes were calculated by normalizing the log2-ratios of RPA-ChIP-reads mapping to forward and reverse strand in 50 bp bins for chromosome length. Data are representative of n=2 biological replicates.

(e) and (g) Stalled replication forks cause a differential signature of single-stranded DNA accumulating with strand bias around early-replicating origins. RPA-ChIP samples were taken from G1-arrested *wild-type* cells released to S-phase in the presence of 200 mM HU for the indicated times. (f) Read asymmetry (as in (d), plotted as mean (dark) ± SD (light)) was averaged over full-length chromosomes and shows no strand bias. (g) Read asymmetry (as in (d)/(f), plotted as mean (dark) ± SD (light)) but averaged around early- and late-replicating origins (autonomously replicating sequences (ARS)) ± 20 Kb shows a minor strand bias close to replication origins consistent with exposure of ssDNA during lagging strand synthesis.

(h) Asymmetric accumulation of RPA (indicating single-stranded DNA) occurs on both long and short chromosomes. Single-stranded DNA (ssDNA) asymmetry scores for individual chromosomes were calculated for the data in Fig. 5b-g by normalizing log2-ratios of RPA-ChIP-reads mapping to forward and reverse strand at the indicated timepoints in 50 bp bins for chromosome length. Data are representative of n=2 biological replicates.

(i) Early firing origins are preferentially located close to the chromosome midpoint and have a slight skew toward the right part of chromosomes. The distances of either all or the 50 earliest-firing origins from the arithmetic midpoint of each chromosome were plotted as an empirical cumulative density function. Dotted lines indicate the chromosome midpoint (vertical) and the 50% fraction (horizontal).

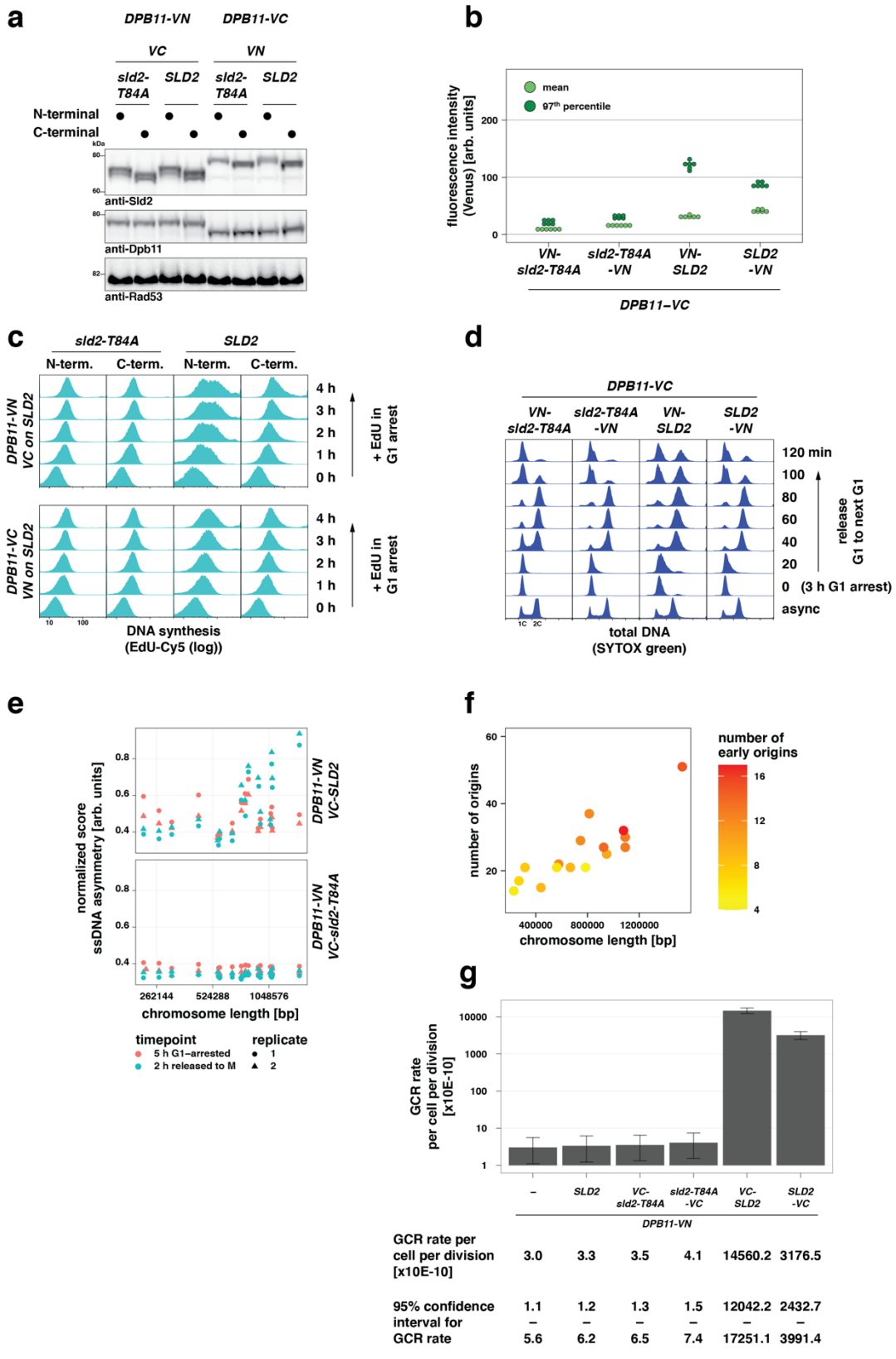

GCR rate per cell per division [x10E-10]	3.0	3.3	3.5	4.1	14560.2	3176.5
95% confidence interval for GCR rate	1.1 – 5.6	1.2 – 6.2	1.3 – 6.5	1.5 – 7.4	12042.2 – 17251.1	2432.7 – 3991.4

Supplementary Figure 7

Low levels of sporadic G1 replication generate head-to-tail fork collisions and genome instability

(a) Split-Venus tagged Dpb11- and Sld2-constructs are expressed to similar levels. Expression levels of Sld2 and Dpb11 carrying split-Venus tags as well as phosphorylated Rad53 detected by western blots from log-phase samples. Note the faint signal for phosphorylated Rad53 with constructs that stabilize the physical interaction between Dpb11 and Sld2 (*VC-SLD2* and *VN-SLD2*).

(b) Split-Venus tags (VN/VC) stabilize the physical interaction between Dpb11 and Sld2. Dpb11-VC and Sld2 tagged at either N- or C-terminus with VN-fragment of the fluorescent protein Venus. Mean (light green) and 97th percentile (dark green) of split-Venus fluorescence intensity were measured by flow cytometry in log-phase cells. Data from n=6 biological replicates.

(c) Venus-stabilized interaction of Dpb11 and Sld2 induces DNA replication in G1. Cells of the indicated genotypes were pre-arrested in G1 for 1 h and then kept arrested in G1 in the presence of EdU (100 μM). Incorporated EdU was labeled with Cy5 and measured by flow cytometry. Note the logarithmic scale of the x-axis to resolve different amounts of G1 replication. Data are representative of n=2 biological replicates.

(d) Venus-stabilized interaction of Dpb11 and Sld2 results in cell cycle arrest. Additional samples to experiment shown in Fig. 6b. SYTOX green-stained total DNA from samples at the indicated timepoints after release from G1 arrest to the next G1-phase as measured by flow cytometry.

(e) Sporadic G1 replication affects long chromosomes more strongly. Single-stranded DNA (ssDNA) asymmetry scores for individual chromosomes were calculated by normalizing the log2-ratios of RPA-ChIP-seq reads mapping to forward and reverse strand in 50 bp bins for chromosome length. Data are representative of n=2 biological replicates.

(f) Long chromosomes harbor more early-firing origins. Length of chromosomes was plotted against the total number of ARS sequences. Color intensity indicates the number of early-firing origins.

(g) High levels of genome instability are caused by Venus-stabilized interaction of Dpb11 and Sld2. GCR rates (median) for the assay shown in Fig. 6f were calculated from n=8 cultures by fluctuation analysis. Error bars indicate a 95% confidence interval for the determined GCR rate. Note the logarithmic scaling of the y-axis.

Source data are provided as a Source Data file.

Fig. 4b (Rad53)

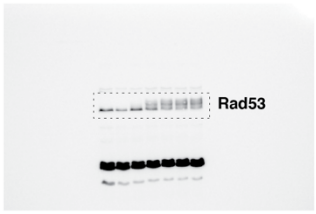

Fig. 4b (γH2A)

Supp. Fig. 4b (γH2A)
same image as Fig. 4b
levels adjusted to show weaker bands

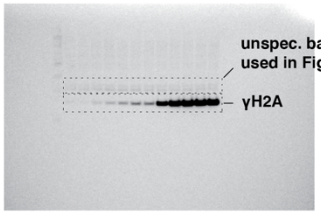

Fig. 4d (Rad53, control)

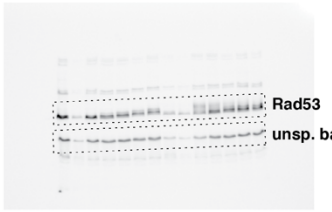

Fig. 4d (Rad53, CDK/DDK bypass)

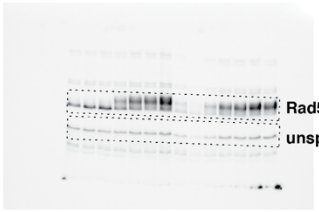

Fig. 4d (γH2A, control)

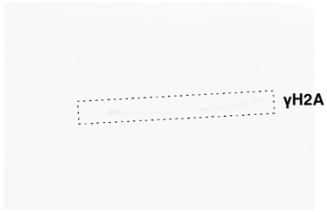

Fig. 4d (γH2A, CDK/DDK bypass)

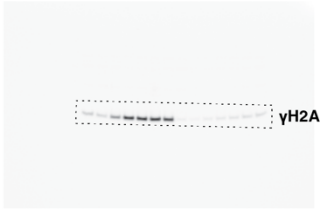

Fig. 4f (Rad53, control)

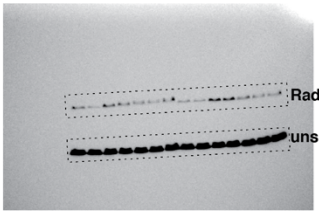

Fig. 4f (Rad53, CDK/DDK bypass)

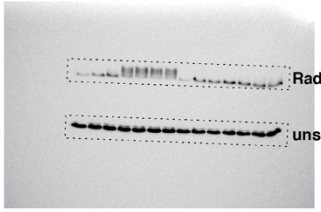

Fig. 4f (γH2A)

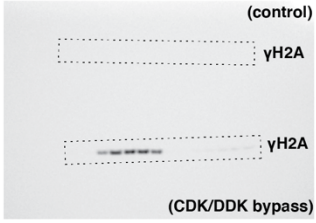

Supp. Fig. 4d (γH2A, control)

Supp. Fig. 4d (γH2A, CDK/DDK bypass)

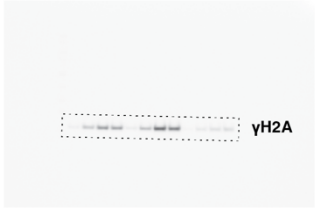

Supp. Fig. 4d (Rad53, control)

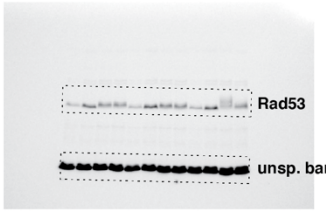

Supp. Fig. 4d (Rad53, CDK/DDK bypass)

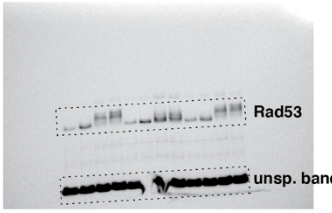

Supp. Fig. 4f (Rad53, no drug)

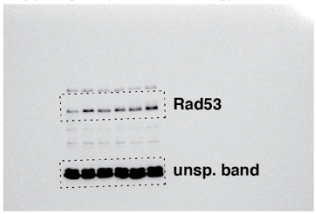

Supp. Fig. 4f (Rad53, 200 mM HU)

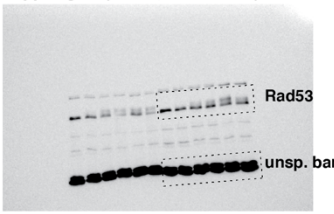

Supp. Fig. 4f (Rad53, 0.005% MMS)

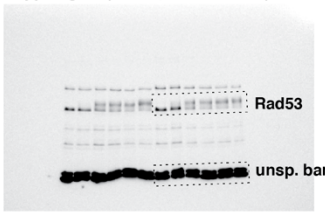

Supp. Fig. 4f (γH2A, no drug)

Supp. Fig. 4f (γH2A, 200 mM HU)

Supp. Fig. 4f (γH2A, 0.005% MMS)

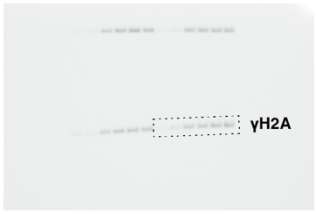

Supp. Fig. 4h (Rad53, control)

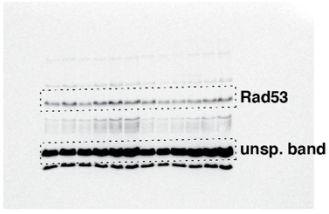

Supp. Fig. 4h (Rad53, CDK/DDK bypass)

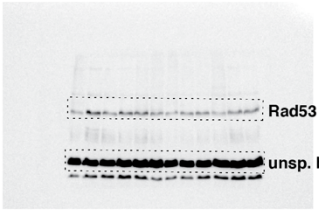

Supp. Fig. 4h (γH2A, control)

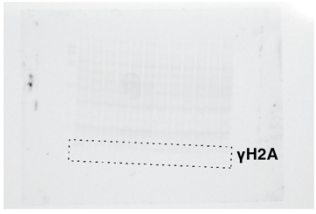

Supp. Fig. 4h (γH2A, CDK/DDK bypass)

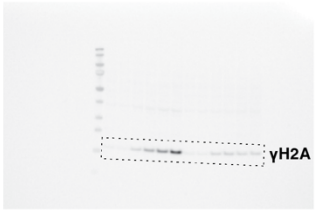

Fig. 6c (Rad53, SLD2-VC)

Fig. 6c (Rad53, sld2-T84A-VC)

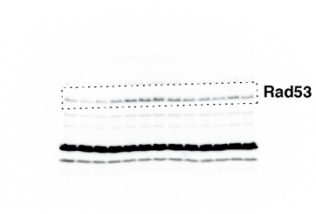

Fig. 6c (Rad53, VC-SLD2)

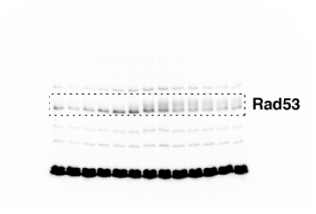

Fig. 6c (Rad53, VC-sld2-T84A)

Supp. Fig. 7a (Sld2)

Supp. Fig. 7a (Dpb11)

Supp. Fig. 7a (Rad53)

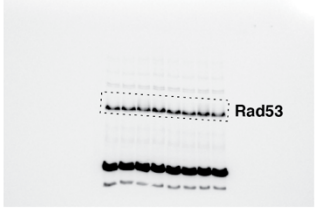

Supplementary Figure 8
Uncropped images of all western blots
Boxes indicate the bands shown in the other figures.

Supplementary Tables

Supplementary Table 1: Budding yeast strains used in this study

strain	genotype	source / reference
W303-1A	*MAT**a** ade2-1 ura3-1 his3-11,15 trp1-1 leu2-3,112 can1-100*	(Rothstein, 1983)
E3087	W303-1A *RAD5+ ura3::URA3/pGPD-TK(5x) AUR1c::pADH-hENT1*	(Talarek et al., 2015)
YKR1445	*leu2::pGAL-DPB11/sld2-T84D::LEU2*	this study
YKR1447	*his3::pGAL-DBF4::HIS3 leu2::pGAL-DPB11/sld2-T84D::LEU2*	this study
YKR1500	*AUR1c::pADH-hENT1 bar1Δ::natNT2*	this study
YKR1501	*leu2::pGAL-DPB11/SLD2::LEU2 bar1Δ::natNT2*	this study
YKR1502	*leu2::pGAL-DPB11/sld2-T84D::LEU2 bar1Δ::natNT2*	this study
YKR1503	*his3::pGAL-DBF4::HIS3 leu2::pGAL-DPB11/sld2-T84D::LEU2 bar1Δ::natNT2*	this study
YKR1546	*pep4Δ::kanMX4*	this study
YKR1558	*pep4Δ::kanMX4 PSF2-yeGFP::hphNT1*	this study
YKR1553	*pep4Δ::kanxM4 his3::pGAL-DBF4::HIS3 leu2::pGAL-DPB11/sld2-T84D::LEU2 bar1Δ::natNT2*	this study
YKR1557	*pep4Δ::kanxM4 his3::pGAL-DBF4::HIS3 leu2::pGAL-DPB11/sld2-T84D::LEU2 bar1Δ::natNT2 PSF2-yeGFP::hphNT1*	this study
YKR1549	*pep4Δ::kanMX4 his3::pGAL-DBF4::HIS3 leu2::pGAL-DPB11/sld2-T84D::LEU2*	this study
YKR1615	*pep4Δ::kanMX4 his3::pGAL-DBF4::HIS3 leu2::pGAL-DPB11/sld2-T84D::LEU2 PSF2-yeGFP::hphNT1*	this study
YKR1815	*leu2::pGAL-DPB11/sld2-T84D::LEU2 bar1Δ::natNT2 his3::pGAL-DBF4/SLD3::HIS3 trp1::pGAL-CDC45/SLD7::TRP1*	this study
YKR2113	*leu2::pGAL-DPB11/sld2-T84D::LEU2 bar1Δ::natNT2 his3::pGAL-DBF4::HIS3 trp1::pGAL-JET1::TRP1*	this study
YKR2114	*leu2::pGAL-DPB11/sld2-T84D::LEU2 bar1Δ::natNT2 his3::pGAL-DBF4/SLD3::HIS3 trp1::pGAL-JET1/SLD7::TRP1*	this study

YKR2035	*leu2::pGAL-DPB11/sld2-T84D::LEU2* *bar1Δ::natNT2* *his3::pGAL-DBF4/SPT21-3FLAG::HIS3*	this study
YKR2090	*his3::pGAL-DBF4::HIS3* *leu2::pGAL-DPB11/sld2-T84D::LEU2* *bar1Δ::natNT2* *cdc45::JET1::TRP1*	this study
YKR2108	*leu2::pGAL-DPB11/sld2-T84D::LEU2* *bar1Δ::natNT2* *cdc45::JET1::TRP1* *his3::pGAL-DBF4/SPT21-3FLAG::HIS3*	this study
YKR1603	*leu2::pGAL-DPB11/sld2-T84D::LEU2* *bar1Δ::natNT2* *his3::pGAL-dbf4-RxxL-4A (R10A,L13A,R62A,L65A)::HIS3*	this study
YKR1563	*his3::pGAL-DBF4::HIS3* *leu2::pGAL-DPB11/sld2-T84D::LEU2* *bar1Δ::natNT2* *rif1Δ::hphNT1*	this study
YKR1803	*his3::pGAL-DBF4::HIS3* *leu2::pGAL-DPB11/sld2-T84D::LEU2* *bar1Δ::natNT2* *sml1Δ::hphNT1* *dif1Δ::kanMX4*	this study
YKR1614	*leu2::pGAL-DPB11/sld2-T84D::LEU2* *his3::pGAL-DBF4/RNR1::HIS3* *bar1Δ::natNT2*	this study
YKR1824	*leu2::pGAL-DPB11/sld2-T84D::LEU2* *bar1Δ::natNT2* *his3::pGAL-DBF4/rnr1-D57N::HIS3*	this study
YKR2099	*his3::pGAL-DBF4::HIS3* *leu2::pGAL-DPB11/sld2-T84D::LEU2* *bar1Δ::natNT2* *trp1::pGAL-CDC6::TRP1*	this study
YKR2059	*trp1::pTDH3-TIR1-9myc,tTA,tetR'-SSN6::TRP1* *SLD3::(hphNT1)iAID-promoter-sld3-3aid*-9myc::natNT2*	this study
YKR2067	*leu2::pGAL-DPB11/sld2-T84D::LEU2* *his3::pGAL-DBF4::HIS3* *trp1::pTDH3-TIR1-9myc,tTA,tetR'-SSN6::TRP1* *SLD3::(hphNT1)iAID-promoter-sld3-3aid*-9myc::natNT2*	this study
YKR1538	*trp1::DDC1-RAD9-3FLAG::TRP1*	this study
YKR1541	*his3::pGAL-DBF4::HIS3* *leu2::pGAL-DPB11/sld2-T84D::LEU2* *trp1::DDC1-RAD9-3FLAG::TRP1*	this study
YKR1564	*trp1::DDC1-RAD9-3FLAG::TRP1* *bar1Δ::natNT2*	this study
YKR1567	*his3::pGAL-DBF4::HIS3* *leu2::pGAL-DPB11/sld2-T84D::LEU2* *trp1::DDC1-RAD9-3FLAG::TRP1* *bar1Δ::natNT2*	this study
YKR2025	*rad9Δ::hphNT1*	this study
YKR2026	*mrc1Δ::hphNT1*	this study
YKR1484	*his3::pGAL-DBF4::HIS3* *leu2::pGAL-DPB11/sld2-T84D::LEU2* *rad9Δ::hphNT1*	this study

YKR1481	*his3::pGAL-DBF4::HIS3* *leu2::pGAL-DPB11/sld2-T84D::LEU2* *mrc1Δ::hphNT1*	this study
YKR1996	*trp1::pGPD-TIR1-3myc::TRP1* *cdc6-3aid*-9myc::natNT2*	this study
YKR2000	*trp1::pGPD-TIR1-3myc::TRP1* *leu2::pGAL-DPB11/sld2-T84D::LEU2* *his3::pGAL-DBF4::HIS3* *cdc6-3aid*-9myc::natNT2*	this study
YKR1754	*ARS702::[I-SceI-cut site]::TRP1*	this study
YKR1755	*leu2::pGAL-DPB11/sld2-T84D::LEU2* *ARS702::[I-SceI-cut site]::TRP1*	this study
YKR1756	*his3::pGAL-DBF4::HIS3* *leu2::pGAL-DPB11/sld2-T84D::LEU2* *ARS702::[I-SceI-cut site]::TRP1*	this study
YKR1642	*rad52Δ::hphNT1*	this study
YKR1645	*his3::pGAL-DBF4::HIS3* *leu2::pGAL-DPB11/sld2-T84D::LEU2* *rad52Δ::hphNT1*	this study
YKR1737	*leu2::pADH-DPB11-VN::LEU2*	this study
YKR1768	*leu2::pADH-DPB11-VN::LEU2* *trp1::pADH-VC-sld2-T84A::TRP1*	this study
YKR1832	*leu2::pADH-DPB11-VN::LEU2* *trp1::pADH-sld2-T84A-VC::TRP1*	this study
YKR1767	*leu2::pADH-DPB11-VN::LEU2* *trp1::pADH-VC-SLD2::TRP1*	this study
YKR1831	*leu2::pADH-DPB11-VN::LEU2* *trp1::pADH-SLD2-VC::TRP1*	this study
YKR1830	*leu2::pADH-DPB11-VC::LEU2*	this study
YKR1836	*leu2::pADH-DPB11-VC::LEU2* *trp1::pADH-VN-sld2-T84A::TRP1*	this study
YKR1834	*leu2::pADH-DPB11-VC::LEU2* *trp1::pADH-sld2-T84A-VN::TRP1*	this study
YKR1835	*leu2::pADH-DPB11-VC::LEU2* *trp1::pADH-VN-SLD2::TRP1*	this study
YKR1833	*leu2::pADH-DPB11-VC::LEU2* *trp1::pADH-SLD2-VN::TRP1*	this study
YKR1763	W303-1A *CAN1::URA3* *leu2::pADH-DPB11-VN::LEU2*	this study
YKR1783	W303-1A *CAN1::URA3* *leu2::pADH-DPB11-VN::LEU2* *trp1::pADH-SLD2::TRP1*	this study
YKR1780	W303-1A *CAN1::URA3* *leu2::pADH-DPB11-VN::LEU2* *trp1::pADH-VC-SLD2::TRP1*	this study
YKR1781	W303-1A *CAN1::URA3* *leu2::pADH-DPB11-VN::LEU2* *trp1::pADH-VC-sld2-T84A::TRP1*	this study
YKR1850	W303-1A *CAN1::URA3* *leu2::pADH-DPB11-VN::LEU2* *trp1::pADH-SLD2-VC::TRP1*	this study

YKR1851	W303-1A *CAN1::URA3* *leu2::pADH-DPB11-VN::LEU2* *trp1::pADH-sld2-T84A-VC::TRP1*	this study

Supplementary Table 2: Plasmids used in this study

plasmid name	vector	insert
pKR588	pFA6a-natNT2	*3aid*-9myc*
pKR534	YIplac128	*pGAL-DPB11/SLD2*
pKR535	YIplac128	*pGAL-DPB11/sld2-T84D*
pKR520	pRS303	*pGAL-DBF4*
pKR546	pRS303	*pGAL-DBF4/SLD3*
pKR581	YIplac204	*pGAL-CDC45/SLD7*
pKR609	YIplac204	*pGAL-JET1/SLD7*
pKR608	YIplac204	*pGAL-JET1*
pKR598	pRS303	*pGAL-SPT21-3FLAG*
pKR592	pRS303	*pGAL-DBF4/SPT21-3FLAG*
pKR604	YIplac204	*pGAL-PRI1/PRI2*
pKR614	pRS303	*pGAL-POL1-3FLAG/POL12*
pKR531	pRS303	*pGAL-dbf4ΔD-box*
pKR563	pRS303	*pGAL-RNR1*
pKR582	pRS303	*pGAL-rnr1-D57N*
pKR562	pRS303	*pGAL-DBF4/RNR1*
pKR583	pRS303	*pGAL-DBF4/rnr1-D57N*
pKR508	YIplac204	*pGAL-CDC6*
pKR548	pRS304	*pGPD-TIR1-3myc*
pKR385	YIplac128	*pADH-DPB11-VN*
pKR386	YIplac128	*pADH-DPB11-VC*
pKR477	YIplac204	*pADH-SLD2*
pKR417	YIplac204	*pADH-VC-SLD2*
pKR425	YIplac204	*pADH-VC-sld2-T84A*
pKR403	YIplac204	*pADH-SLD2-VC*
pKR413	YIplac204	*pADH-sld2-T84A-VC*
pKR416	YIplac204	*pADH-VN-SLD2*
pKR424	YIplac204	*pADH-VN-sld2-T84A*
pKR402	YIplac204	*pADH-SLD2-VN*
pKR412	YIplac204	*pADH-sld2-T84A-VN*

Supplementary Table 3: Fold changes of individual replisome proteins

id	genes	complex	LFQ G1_1	LFQ G1_2	LFQ G1_3	LFQ S_1	LFQ S_2	LFQ S_3	mean LFQ G1	mean LFQ S	fold change S vs G1	p-value
P40359	PSF2	GINS and CTF4	37.857	38.068	38.269	37.943	37.760	37.852	37.852	38.065	-0.213	0.17734
Q01454	CTF4	GINS and CTF4	39.443	39.456	39.641	39.099	39.027	39.257	39.128	39.513	-0.386	0.01456
Q03406	SLD5	GINS and CTF4	38.440	38.282	38.764	38.012	38.086	38.175	38.091	38.496	-0.405	0.05386
Q12146	PSF3	GINS and CTF4	37.505	37.600	37.110	37.074	37.066	36.485	36.875	37.405	-0.530	0.09762
Q12488	PSF1	GINS and CTF4	38.108	37.949	37.853	37.593	37.456	37.810	37.620	37.970	-0.351	0.05097
P24279	MCM3	CMG helicase	34.585	34.824	35.174	37.001	37.067	36.797	36.955	34.861	2.094	0.00038
P29469	MCM2	CMG helicase	34.357	34.169	34.596	36.597	36.987	36.893	36.826	34.374	2.452	0.00014
P29496	MCM5	CMG helicase	34.729	34.210	34.005	37.063	36.840	36.706	36.870	34.315	2.555	0.00044
P30665	MCM4	CMG helicase	35.145	34.891	35.110	37.366	37.150	37.322	37.279	35.049	2.230	0.00003
P38132	MCM7	CMG helicase	34.661	34.346	34.574	36.786	36.846	36.768	36.800	34.527	2.273	0.00002
P53091	MCM6	CMG helicase	35.001	34.633	34.829	36.960	37.223	37.071	37.085	34.821	2.263	0.00007
Q08032	CDC45	CMG helicase	32.307	33.600	32.897	35.956	35.797	35.989	35.914	32.935	2.979	0.00140
P21951	POL2	pol epsilon	32.788	32.120	32.599	34.060	34.697	33.908	34.221	32.502	1.719	0.00534
P24482	DPB2	pol epsilon	30.662	30.119	29.762	32.205	32.428	32.767	32.467	30.181	2.286	0.00176
P27344	DPB3	pol epsilon	29.727	29.220	29.802	30.097	30.667	30.219	30.328	29.583	0.745	0.04171
Q04603	DPB4	pol epsilon	29.726	29.837	30.183	31.457	31.945	31.513	31.638	29.916	1.723	0.00113
P10363	PRI1	pol alpha / primase	28.871	28.506	28.624	32.224	32.179	31.996	32.133	28.667	3.466	0.00001
P13382	POL1	pol alpha / primase	28.540	27.143	28.434	33.835	33.941	33.609	33.795	28.039	5.756	0.00023
P20457	PRI2	pol alpha / primase	24.065	23.399	23.569	31.288	31.523	31.316	31.376	23.678	7.698	0.00000
P38121	POL12	pol alpha / primase	28.442	26.615	28.222	32.713	32.417	32.267	32.466	27.760	4.706	0.00134
P04786	TOP1	repl.-associated factors	31.623	31.409	31.859	34.777	35.013	34.529	34.773	31.630	3.143	0.00008
P25588	MRC1	repl.-associated factors	34.933	35.119	34.831	37.110	37.461	37.594	37.388	34.961	2.427	0.00013
P32354	MCM10	repl.-associated factors	25.877	24.068	26.211	29.164	29.428	28.991	29.194	25.385	3.809	0.00493
P32558	SPT16	repl.-associated factors	34.877	34.614	34.738	36.865	37.072	36.909	36.949	34.743	2.206	0.00002
P38766	RRM3	repl.-associated factors	29.864	29.483	29.512	31.954	32.803	31.835	32.197	29.619	2.578	0.00143
P52286	SKP1	repl.-associated factors	32.071	31.549	31.974	33.118	33.277	33.071	33.155	31.865	1.291	0.00169
P53840	TOF1	repl.-associated factors	34.278	32.848	34.288	36.187	37.057	36.724	36.656	33.805	2.851	0.00622
Q04636	POB3	repl.-associated factors	33.510	33.260	33.717	35.748	35.763	35.759	35.757	33.496	2.261	0.00007
Q04659	CSM3	repl.-associated factors	31.244	31.570	31.816	34.122	34.172	33.994	34.096	31.543	2.553	0.00013
Q08273	HRT1	repl.-associated factors	30.268	30.085	30.549	32.061	32.487	32.454	32.334	30.301	2.033	0.00045
Q08496	DIA2	repl.-associated factors	33.399	32.530	32.779	35.750	35.965	35.351	35.689	32.903	2.786	0.00090
Q12018	CDC53	repl.-associated factors	32.641	32.967	33.335	35.063	35.322	35.407	35.264	32.981	2.283	0.00054